Synchronous Push–Pull Class E Rectifiers With Load-Independent Operation for Megahertz Wireless Power Transfer

Xiaosheng Huang, *Member, IEEE*, Yi Dou, *Graduate Student Member, IEEE*, Shuyi Lin, Yuan Tian, Ziwei Ouyang, *Senior Member, IEEE*, and Michael A. E. Andersen, *Member, IEEE*

***Abstract*—This article presents the analytical modeling of synchronous class E rectifiers with the load-independent operation, which achieves zero-phase-angle input impedance, soft-switching over the entire load range with a constant voltage gain. The optimal design of the synchronous class E rectifier is proposed to realize both zero-voltage-switching turn-ON and zero-current-switching turn-OFF at the expected output power. An LCC-S compensated MHz-WPT topology, which comprises the push–pull class E inverter and rectifier with the load-independent operation, is proposed to achieve the fully soft-switching and a nearly constant voltage gain over the entire load range. The efficiency improvement of the compensation network is also investigated to provide a design methodology for the proposed topology. A 6.78-MHz WPT prototype, along with an alternative phase detector using an auxiliary coil to realize phase detection, is built to validate the analytical model and the proposed methodology. The system efficiency reaches 86.7% at 214-W output. The synchronous push–pull class E rectifier maintains soft-switching over the load range, and the rectification efficiency reaches 94.6%.**

***Index Terms*—Class E, load independent, synchronous rectifier, wireless power transfer (WPT).**

NOMENCLATURE

ω	Angular frequency.
i_{ac}	Input current of rectifier.
I_{ac}	Amplitude of i_{ac}.
v_{ac}	Input voltage of a rectifier.
V_{ac}	Amplitude of v_{ac}.
φ	Phase shift of i_{ac}.
v_S	Switch voltage.
v_{Sn}	$= \frac{v_S}{V_{\text{dc}}}$. Normalized switch voltage.
i_S	Switch current.
i_{Sn}	$= \frac{i_S}{I_{\text{dcr}}}$. Normalized switch current.
i_{Lf}	Current passing through L_f.
$I_{L\pi}$	Current passing through L_f at $\omega t = \pi$.
p_π	$= \frac{I_{L\pi}\cdot\omega L_f}{V_{\text{dc}}}$. Normalized $I_{L\pi}$.
q	$= \frac{1}{\omega\sqrt{L_f C_f}}$. Normalized resonant frequency of L_f and C_f.
p	$= \frac{I_{\text{ac}}\cdot\omega L_f}{V_{\text{dc}}}$. Load factor of a rectifier.
p_{optm}	Optimal rated value of p.
R_{optm}	Load resistance mapping to p_{optm}.
R_r	Rated load resistance of a rectifier.
G_{rec}	Voltage gain of a rectifier.
I_{dcr}	Rated output current of a rectifier.
P_{or}	Rated output power of a rectifier.
$G_{\text{rec\_}d}$	Voltage gain of a push–pull rectifier.
$G_{\text{inv\_}d}$	Voltage gain of a push–pull inverter.
G_{mag}	Voltage gain of a resonant tank.
P_{o_d}	Output power of a push–pull rectifier.
$P_{\text{or\_}d}$	Rated output power of a push–pull rectifier.
R_{r_d}	Rated load resistance of a push–pull rectifier.
k_{23}	Coupling coefficient between L_2 and L_3.
k_{tr}	Coupling coefficient between L_t and L_r.
k_{eq}	$= \sqrt{L_1/L_2}$. Equivalent coupling coefficient between loop_1 and loop_2 of a resonant tank.
$R_{1\sim3}$	ESR of resonance $\text{loop}_{1\sim3}$.
$Q_{1\sim3}$	$= \frac{\omega L_{1\sim3}}{R_{1\sim3}}$. Resonant quality factors of $\text{loop}_{1\sim3}$.
Q_L	$= \frac{\omega L_3}{R_{\text{ac}}}$. Loaded quality factor of a resonant tank.
R_{dco}	Load resistance of a receiver.

Manuscript received June 30, 2020; revised September 25, 2020; accepted November 11, 2020. Date of publication November 17, 2020; date of current version February 5, 2021. This work was supported in part by the National Natural Science Foundation of China under Grant 51607039, in part by the Natural Science Foundation of Fujian Province of China under Grants 2019J01772 and 2018J01623, and in part by the Program for the Training of Distinguished Young Scientists in Fujian Provincial Universities under Grant GY-Z18161. Recommended for publication by Associate Editor C. Fernandez. *(Corresponding author: Ziwei Ouyang.)*

Xiaosheng Huang, Shuyi Lin, and Yuan Tian are with the School of Electronic, Electrical Engineering and Physics, Fujian University of Technology, Fuzhou 350118, China (e-mail: hxs@fjut.edu.cn; linshuyi1985@qq.com; tianyuan8162@qq.com).

Yi Dou, Ziwei Ouyang, and Michael A. E. Andersen are with the DTU Elektro, Technical University of Denmark, 2800 Kongens Lyngby, Denmark (e-mail: yidou@elektro.dtu.dk; zo@elektro.dtu.dk; ma@elektro.dtu.dk).

Color versions of one or more of the figures in this article are available at https://doi.org/10.1109/TPEL.2020.3038814..

Digital Object Identifier 10.1109/TPEL.2020.3038814

I. INTRODUCTION

WIRELESS power transfer (WPT) is getting more attractive for the applications of power electronics (e.g., portable devices, medical implants, electric vehicles, etc.) [1]–[5]. For WPT systems based on magnetic coupling, increasing operation frequency usually means smaller magnetic components and higher induced voltage. It is conducive to reduce the system size, extend the transfer distance, and enhance misalignment tolerance. However, the increased frequency brings a

challenge to high-efficiency and high-reliable MHz-WPT systems because of the substantial losses of the switches and the resonant tank. Up to now, the issues on high-frequency rectifiers are attracting more attention as the rectification loss constitutes a large portion of the system losses [6]–[13].

Various topologies can realize the high-frequency rectification, such as full-bridge [14], class E [15], class DE [16], class EF [17], and class F [18]. Due to the increased switching losses, the rectification efficiency may distinctly reduce when working in the MHz region. Moreover, the parasitic inductance and capacitance may cause serious ringing (i.e., high-frequency harmonics) at the instant of switching. This phenomenon not only leads to additional losses but also results in electromagnetic interference issues. Therefore, the soft-switching resonant rectifiers are required to overcome the above-mentioned issues.

Class E resonant rectifiers are attractive for MHz-WPT applications due to its simplicity and low harmonic contents [19]. The conventional half-wave class E rectifiers can achieve low-voltage-derivation switching (i.e., the diode turns OFF at zero dv_D/dt and turns ON at low dv_D/dt) by using a capacitor in parallel with the diode [20], [21]. A similar approach can be implemented to achieve low-current-derivation switching (i.e., the diode turns ON at zero di_D/dt and turns OFF at low di_D/dt) by using an inductor in series with the diode [22]. Besides, the harmonic contents can be further reduced by interleaving two half-wave rectifiers, which constitute a full-wave class E rectifier. Both of the class E half-wave and full-wave rectifiers for MHz-WPT systems were discussed [7], [9]. However, the inherent forward voltage of diodes will cause high conducting losses, which limit the applications of class E rectifiers.

The synchronous rectification is a promising way to reduce the losses caused by diode-based rectifiers. Class E and its derivative topologies (e.g., class EF and push–pull class E), which comprise only low-side-driven switches, are preferred for MHz-WPT systems. Different from the diodes that block the reverse current, the synchronous switches are able to conduct bidirectionally. Thus, the synchronous rectifiers can operate as time-reversed inverters. Synchronous class E rectifiers can be found in many dc–dc converters with the operation frequency from kHz to GHz [23]–[27]. However, so far, there are few articles those discussed the synchronous class E rectifiers for MHz-WPT systems, of which the resonant tank is different from that of conventional dc–dc converters [8]–[13].

The phase shift control is usually required to achieve soft-switching of synchronous rectifiers by adjusting the switching phase over the load range [10]. Generally, two kinds of methods can directly realize the phase detection, i.e., the voltage-comparator-based [8] and the current-transformer-based [9], [10]. As in [8], a voltage comparator is implemented to detect the threshold of the switch voltage and generate a fixed-width pulse. However, the waveform of the switch voltage changes as the load varies, and results in an unexpected switching phase shift. This issue will be more troublesome in the differential (i.e., push–pull) class E topology due to the unbalance voltage waveforms [28]. In [9], the zero-current detection is implemented to generate the gate driving signal of several hundred kHz. However, it is challenging for the existing current transformers to work in the MHz region due to the bandwidth limitation. The self-oscillating resonant gate driver is another potential solution to drive the synchronous switches [24]. However, the switching phase is also sensitive to the load variation since the driver is energized by an alternating voltage node of the rectifier.

The existing studies still lack a preferable method to drive the synchronous switches avoiding the unexpected phase shift caused by the load variation. Consequently, the load-independent class E rectifiers are preferable to simplify the control since the optimal switching phase is constant. Theoretically, the parameters of the synchronous rectifiers are identical with that of the inverters. However, modeling the load-independent operation from the perspective of inversion cannot provide a concise method to obtain the impedance features and the circuit parameters of load-independent class E rectifiers. The rectification efficiency and the voltage gain are highly dependent on the impedance features, which are related to load variation. Due to the lack of detailed analytical modeling in the existing literature, it is difficult to analyze and optimize the load-independent synchronous class E rectifiers for MHz-WPT applications.

This article investigates the analytical modeling of synchronous class E rectifiers with the load-independent operation from the perspective of rectification. It provides a straightforward method to analyze and design the load-independent synchronous class E rectifiers. Based on the model, the implementation for the proposed MHz-WPT topology is also presented. Section II presents the detailed analytical derivation of the single-switch synchronous class E rectifiers with the load-independent operation, which achieves both zero-phase-angle (ZPA) input and soft-switching over the entire load range with a constant voltage gain. The optimal design is proposed according to the analytical expressions deducted. Then, Section III proposes an LCC-S compensated MHz-WPT topology combined with the load-independent push–pull synchronous class E rectifier, which is derived from the single-switch one. The improved design method of the compensation network is also investigated to provide a design methodology for the proposed topology. In Section IV, a design example is presented and simulated. Then, in Section V, the hardware implementation is also illustrated regarding the inverter, the rectifier, the compensation network, and the phase detector avoiding the unexpected phase shift of conventional methods. The 6.78-MHz WPT prototype is built and tested to validate the analytical model and the optimization method proposed. Finally, the conclusion is given in Section VI.

II. Analytical Modeling and Design Optimization of Load-Independent Synchronous Class E Rectifiers

The concept of load-independent class E inverters was introduced in [29]. The modeling of the load-independent synchronous class E rectifiers can begin with the derivation of switch voltage, which is similar to modeling the inverters.

A. Switch Voltage

Fig. 1 illustrates the topology of the synchronous class-E rectifier. It is assumed that the switch has zero ON-resistance and

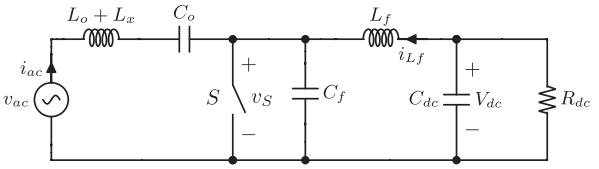

Fig. 1. Synchronous class E rectifier with finite inductance. The output inductor L_f, parallel capacitor C_f, and external inductor L_x construct a load network, which shapes the switch voltage to achieve soft-switching or other features. The input filter (L_o and C_o) resonates at the operation frequency.

infinite OFF-resistance. The switch is ON during $0 < \omega t \leq \pi$ and OFF during $\pi < \omega t \leq 2\pi$. The equivalent series resistance (ESR) of passive components is ignored. The input current, which is filtered by the input filter with high enough $\sqrt{L_o/C_o}$, can be expressed by

$$i_{\text{ac}}(\omega t) = I_{\text{ac}} \cdot \sin(\omega t + \varphi). \tag{1}$$

The ON-state switch current during $0 < \omega t \leq \pi$ is given by

$$i_S(\omega t) = I_{L\pi} + \frac{V_{\text{dc}}}{\omega L} \cdot (\omega t - \pi) + i_{\text{ac}}(\omega t). \tag{2}$$

When the switch is in the OFF-state, C_f is charged by i_{ac} and i_{Lf}. Thus, the switch voltage for $\pi < \omega t \leq 2\pi$ meets

$$\omega C_f \cdot \frac{dv_S}{d\omega t} = \frac{1}{\omega L} \int_{\pi}^{\omega t} (V_{\text{dc}} - v_S) d\omega t + I_{L\pi} + i_{\text{ac}}(\omega t). \tag{3}$$

Differentiating both sides gives

$$\frac{1}{q^2} \frac{d^2 v_{Sn}}{d\omega t^2} - p \cdot \cos(\omega t + \varphi) + v_{Sn} - 1 = 0. \tag{4}$$

Thus, the general solution of the normalized switch voltage is

$$v_{Sn}(\omega t) = 1 + \xi_1 \cos(q\omega t) + \xi_2 \sin(q\omega t) - \xi_3 q \cos(\omega t + \varphi) \tag{5}$$

where

$$\xi_3 = \frac{pq}{1 - q^2}. \tag{6}$$

The coefficients ξ_1 and ξ_2 can be obtained by solving the expressions for zero-voltage-switching (ZVS) turn-OFF, i.e.,

$$v_{Sn}(\pi) = 0 \tag{7}$$

$$\left.\frac{dv_{Sn}(\omega t)}{d\omega t}\right|_{\omega t = \pi} = q^2 p_\pi + q^2 p \cdot \sin(\varphi). \tag{8}$$

Then, ξ_1 and ξ_2 are given by

$$\begin{aligned} \xi_1 = & -\xi_3[\sin(q\pi)\sin(\varphi) + q\cos(q\pi)\cos(\varphi)] \\ & - q\sin(q\pi) \cdot (p_\pi + p\sin(\varphi)) - \cos(q\pi) \\ \xi_2 = & \ \xi_3[\cos(q\pi)\sin(\varphi) - q\sin(q\pi)\cos(\varphi)] \\ & + q\cos(q\pi) \cdot (p_\pi + p\sin(\varphi)) - \sin(q\pi). \end{aligned} \tag{9}$$

Solving the equation for volt–second balance of L_f gives

$$\begin{aligned} p_\pi = & \frac{q\xi_3\cos(\varphi) + 1}{q\tan(\frac{q\pi}{2})^2} + \frac{2q\xi_3\sin(\varphi) + \pi}{2\sin(\frac{q\pi}{2})^2} - \frac{\xi_3\sin(\varphi)}{q} \\ & - p\sin(\varphi). \end{aligned} \tag{10}$$

Consequently, the normalized switch voltage is expressed as a function of three variables, i.e., q, p, and φ.

B. Criteria of Load-Independent Operation

Fourier series can be applied to analyze the voltage gain and input impedance. The fundamental harmonic of v_{Sn} can be separated into the active (V_{Rn}) part and the reactive (V_{Xn}) part given by

$$V_{Rn} = \frac{1}{\pi} \int_{\pi}^{2\pi} v_{Sn}(\omega t)\sin(\omega t + \varphi) d\omega t \tag{11}$$

$$V_{Xn} = \frac{1}{\pi} \int_{\pi}^{2\pi} v_{Sn}(\omega t)\cos(\omega t + \varphi) d\omega t. \tag{12}$$

To figure out the switch voltage with load variation, deriving (11) and (12) with respect to p gives

$$\frac{dV_{Rn}}{dp} = \left[\frac{2q^4\cot(\frac{q\pi}{2})^2}{\pi(q^2-1)^2}\right] \cdot \sin(\varphi)^2 \tag{13}$$

$$\begin{aligned} \frac{dV_{Xn}}{dp} = & \left[\frac{q^4\cos(\varphi)(\cos(q\pi)+1)}{\pi(q^2-1)^2\sin(\frac{q\pi}{2})^2}\right] \cdot \sin(\varphi) \\ & + \frac{2q^3\cot(\frac{q\pi}{2})}{\pi(q^2-1)^2} + \frac{q^2}{2(q^2-1)}. \end{aligned} \tag{14}$$

Let $\varphi = \pi$, (13) and (14) can be simplified as

$$\left.\frac{dV_{Rn}}{dp}\right|_{\varphi=\pi} = 0 \tag{15}$$

which means V_{Rn} is irrelevant to load variation and

$$\xi_4 = \left.\frac{dV_{Xn}}{dp}\right|_{\varphi=\pi} = \frac{2q^3\cot(\frac{q\pi}{2})}{\pi(q^2-1)^2} + \frac{q^2}{2(q^2-1)}. \tag{16}$$

As q is constant for physical rectifiers, V_{Xn} is proportional to the input current. The voltage gain of the rectifier meets

$$\frac{1}{G_{\text{rec}}} = \frac{V_{\text{ac}}}{V_{\text{dc}}} = \left(\xi_4 + \frac{L_x}{L_f}\right) \cdot p + V_{R_n}. \tag{17}$$

Thus, V_{Xn} can be compensated by fixed inductance given by

$$L_x = -\xi_4 L_f. \tag{18}$$

Therefore, by applying the particular values of φ and L_x, the compensated input impedance is purely resistive. A constant load-independent voltage gain is achieved and given by

$$G_{\text{rec}} = \frac{1}{\frac{2}{\pi} + \frac{q}{(1-q^2)\tan(\frac{\pi q}{2})}}. \tag{19}$$

To achieve ZVS turn-ON at $\omega t = 2\pi$, q can be obtained by numerically solving

$$v_{Sn}(2\pi) = 2 + \frac{\sin(q\pi)(q\pi + 2q^2\xi_3\sin(\varphi)}{2\sin(\frac{q\pi}{2})^2} = 0 \tag{20}$$

where $\varphi = \pi$. Thus

$$q = 1.291547. \tag{21}$$

Then, (16) gives

$$\xi_4 = -0.266228. \tag{22}$$

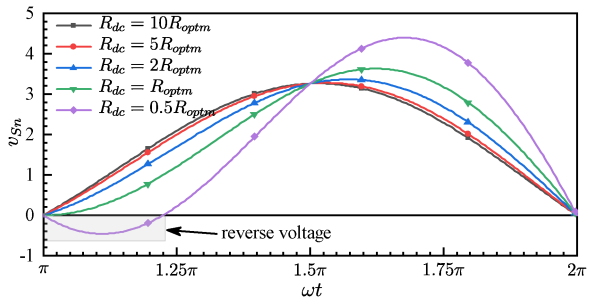

Fig. 2. Normalized switch voltage v_{Sn} versus load resistance $R_{\rm dc}$. ZVS turn-ON is achieved regardless of load variation. The peak voltage increases as $R_{\rm dc}$ decreases. The peak v_{Sn} reaches 4.397 at $R_{\rm dc} = 0.5R_{\rm optm}$, compared with 3.631 at $R_{\rm dc} = R_{\rm optm}$. The reverse voltage usually causes unexpected conducting of physical switches and affect the load-independent operation.

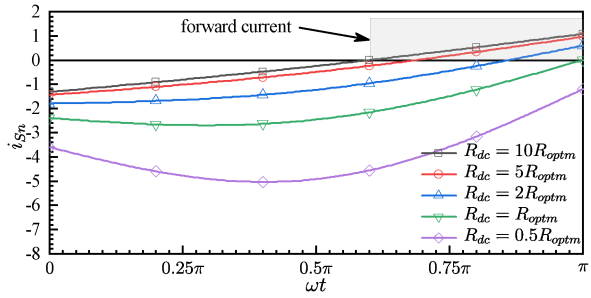

Fig. 3. Normalized switch current i_{Sn} versus load resistance $R_{\rm dc}$. The zero-cross instant moves as load varies. The current amplitude increases as $R_{\rm dc}$ decreases (i.e., the output power increases).

The load-independent voltage gain is given by

$$G_{\rm rec} = 0.629125. \tag{23}$$

Consequently, (21) and (22) give the normalized parameters that are identical for the synchronous class E rectifiers achieving the load-independent operation. It realizes ZVS turn-ON and ZPA input impedance over the entire load range with the constant voltage gain.

C. Design Optimization

In order to design a practical rectifier, the rated parameters have to be calculated to satisfy the required efficiency and the expected output specifications. In this section, an optimal design is proposed to achieve ZVS turn-ON and zero-current-switching (ZCS) turn-OFF at the rated condition, which achieves the maximum efficiency at the expected output power.

The value of p achieving ZCS turn-OFF can be obtained by solving

$$\left.\frac{dv_{Sn}}{d\omega t}\right|_{\omega t=\pi} = \frac{\pi q^2}{2\sin(\frac{q\pi}{2})^2} + q\left(\xi_3+1\right)\cot\left(\frac{q\pi}{2}\right) = 0 \tag{24}$$

which gives the optimal value of p as

$$p_{\rm optm} = 1.648457. \tag{25}$$

According to the definition of p, $p_{\rm optm}$ can be rewritten as

$$p_{\rm optm} = 2G_{\rm rec}\cdot\frac{\omega L_f}{R_{\rm optm}} \tag{26}$$

where $R_{\rm optm}$ is the optimal load resistance mapping to $p_{\rm optm}$. The switch voltage under load variation can be obtained by using different values of p mapping to $R_{\rm dc}$. As shown in Fig. 2, the switch maintains ZVS regardless of load variation. When $R_{\rm dc} < R_{\rm optm}$, the switch will conduct reversely during a specific interval. Normally, the practical switches (MOSFET, GaN FET, etc.) conduct reversely with a limited voltage. Thus, this phenomenon will cause additional switching losses and also affect the voltage gain. Therefore, in this article, we use $R_{\rm optm}$ as the optimal rated $R_{\rm dc}$, i.e., $R_r = R_{\rm optm}$. The synchronous switches can prevent the reverse conducting at OFF-state over the load range from the rated value to infinite.

Consequently, the optimal parameters of a physical rectifier are obtained by

$$R_r = \frac{V_{\rm dc}^2}{P_{\rm or}} \tag{27}$$

$$L_f = \frac{R_r\cdot p_{\rm optm}}{2\omega G_{\rm rec}} \tag{28}$$

$$C_f = \frac{1}{L_f\cdot q^2\omega^2}. \tag{29}$$

Besides, L_X is given by (18). The above equations can realize the load-independent class E rectifiers, which achieve ZPA input impedance and ZVS turn-ON over the entire load range with the constant voltage gain. Moreover, the efficiency is expected to reach the maximum value at the rated condition.

Fig. 3 illustrates i_{Sn} versus $R_{\rm dc}$, where the normalized switch current is expressed as

$$i_{Sn}(\omega t) = \frac{i_S(\omega t)}{I_{\rm dcr}} = \begin{cases} \dfrac{2G_{\rm rec}}{p_{\rm optm}}\cdot p\cdot\sin(\omega t+\varphi) + i_{Lfn}(\omega t) & 0<\omega t\le\pi \\ 0 & \pi<\omega t\le 2\pi \end{cases} \tag{30}$$

where the normalized i_{Lf} is given by

$$i_{Lfn}(\omega t) = \frac{i_{Lf}(\omega t)}{I_{\rm DCr}} = \frac{2G_{\rm rec}}{p_{\rm optm}}\cdot\begin{cases} -\pi+\omega t+p_\pi & 0<\omega t\le\pi \\ p_\pi+\displaystyle\int_\pi^{\omega t}(1-v_{Sn})d\omega t & \pi<\omega t\le 2\pi. \end{cases} \tag{31}$$

As shown in Fig. 3, the direction of the switch current turns into forward during a specific interval. The zero-cross point moves as $R_{\rm dc}$ varies. It means that the zero-crossing-detection of the switch current is not applicable for synchronous switching.

As in Fig. 4, the current amplitude through L_f keeps large over the entire load range. Consequently, the loss of L_f takes a significant part in the total loss of the class E rectifier; which implies that the efficiency will be reduced by using a lower rated value of p (i.e., lower L_f).

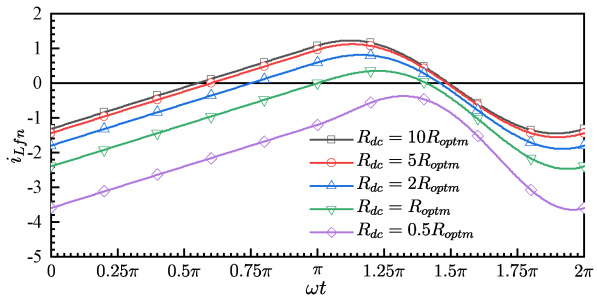

Fig. 4. Normalized inductor current i_{Lfn} versus load resistance $R_{\rm dc}$. The peak–peak value of the current is nearly constant as load varies.

As a result, the optimal circuit parameters of load-independent class E rectifiers, which achieve both ZVS turn-ON and ZCS turn-OFF at the rated load, can be obtained by (18) and (27)–(29).

III. WPT Systems Using Load-Independent Synchronous Push–Pull Class E Rectifier

As analyzed in Section II, the load-independent class E rectifier can realize soft-switching and ZPA input over the entire load range with the constant voltage gain. The features are preferable for the typical MHz-WPT systems to operate at resonant mode and maintain high-efficiency transfer over the load range. However, the single-switch class E rectifier maintains i_{Lf} of large harmonics over the entire load range, and will result in distinctly voltage ripples and electromagnetic interference. As an alternative solution, the push–pull class E topology can be implemented to reduce the voltage ripple and suppress harmonic contents.

This section proposes a MHz-WPT topology, of which the inverter and the rectifier are derived from the load-independent operation analyzed in Section II. As illustrated in Fig. 5, the push–pull class E topology is implemented for both of the inverter and the rectifier to reduce the harmonic contents and increase the power capability. The inverter and the rectifier are connected by the magnetic resonant tank (i.e., the LCC-S compensated coupling coils). Naturally, the voltage gain of the proposed topology can be calculated by

$$G_{\rm wpt} = G_{\rm inv\_}{}_d \cdot G_{\rm mag} \cdot G_{\rm rec\_}{}_d \tag{32}$$

where $G_{\rm inv\_}{}_d$, $G_{\rm mag}$, and $G_{\rm rec\_}{}_d$ are the voltage gains of the push–pull inverter, the resonant tank, and the push–pull rectifier of the WPT system, respectively. The topology of the push–pull class E inverter is symmetric with that of the rectifier, resulting in $G_{\rm inv\_}{}_d = 2G_{\rm rec}$ and $G_{\rm rec\_}{}_d = G_{\rm rec}/2$. Thus, (32) can be simplified as $G_{\rm wpt} = G_{\rm mag}$.

It is worth noting that full-bridge rectifiers are not practicable in the proposed WPT topology. The nonresistive input impedance of the full-bridge rectifier will cause detuning operation of the class E inverter and significantly change the voltage gain. Moreover, it is also difficult to build a 6.78-MHz full-bridge rectifier that can deliver hundreds of watts due to the parasitic ringing and high-harmonic contents.

The proposed WPT topology is well simplified since the first resonant loop acts as an output filter of the inverter, and the third loop acts as an input filter of the rectifier. The external inductance L_x can be integrated with L_1 and L_3 of the compensation network. The analysis and design methodology of the proposed topology are presented in this section as follows.

A. Synchronous Push–Pull Class E Topology With Load-Independent Operation

The push–pull class E rectifier, which comprises two switches operating differentially (i.e., interleaving with 180° shift switching), can naturally eliminate the odd-order harmonics at the output node. Thus, it is conducive to suppress the current ripples through the dc capacitor and reduce the electromagnetic interference [9], [28]. Combined with the load-independent operation, the synchronous push–pull class E rectifier can also achieve ZPA input impedance and soft-switching over the entire load range. The feature of ZPA impedance is promising to realize a high-efficiency transfer as the magnetic resonant tank maintains resonance at the constant frequency over the entire load range.

As shown in Fig. 6, the rectifier input connects to the series-compensated resonant loop. The receiving coil provides the input and external inductance of the rectifier, i.e., L_o and L_x. The switch S_3 is ON during $0 < \omega t \le \pi$ and OFF during $\pi < \omega t \le 2\pi$. In reverse, S_4 is OFF during $0 < \omega t \le \pi$ and ONduring $\pi < \omega t \le 2\pi$. Since the switches operate differentially, the switching behavior is the same as in a single-switch synchronous class E rectifier. Therefore, the aforementioned optimal design methodology is also applicable to realize the load-independent operation for push–pull class E rectifiers. The parameters can be mapped to a single-switch class E rectifier as in Fig. 1, i.e.,

$$R_{r\_d} = \frac{V_{\rm dc}^2}{P_{r\_d}} \tag{33}$$

$$L_{f1,2} = \frac{R_{r\_d} \cdot p_{\rm optm}}{\omega G_{\rm rec}} = 2.620237 \cdot \frac{R_{r\_d}}{\omega} \tag{34}$$

$$C_{f1,2} = \frac{G_{rec}}{R_{r\_d} \cdot p_{\rm optm} q^2 \omega} = 0.228791 \cdot \frac{1}{R_{r\_d} \cdot \omega}. \tag{35}$$

In the proposed WPT topology, the same parameters of the synchronous rectifier (i.e., L_f, L_x, and C_f) are also applied to the inverter. As the synchronous rectifier can be regarded as the time-reversed inverter, the push–pull class E inverter can also achieve the load-independent operation, which achieves soft-switching over the entire load range with a constant voltage gain.

B. Magnetic Resonant Tank of WPT Systems

1) Topology: The resonant tank is formed by the coupling coils and the compensation network. As in Fig. 7, the transmitting coil is compensated by an LCC net. The receiving coil is compensated by a capacitor C_3 in series. Thus, the resonant tank comprises three LC loops resonating at the operation frequency. The parameters meet

$$\frac{1}{\omega^2} = L_1 C_1 = L_2 C_{2\rm eq} = L_3 C_3 \tag{36}$$

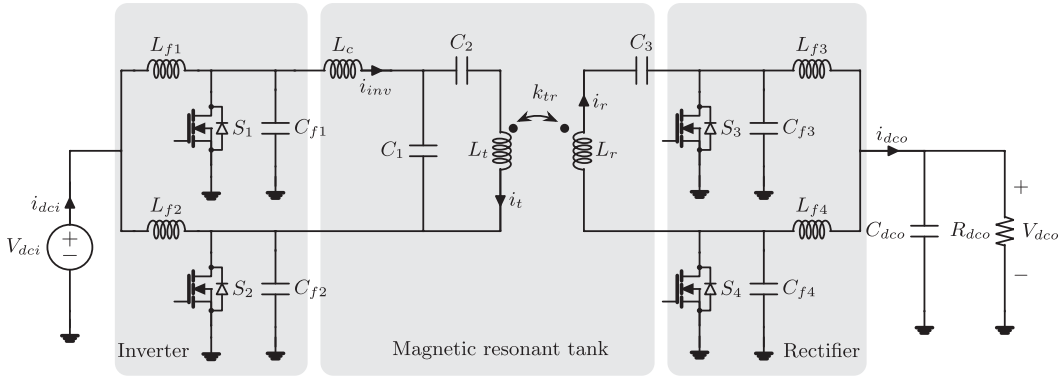

Fig. 5. Proposed WPT topology using the push–pull class E inverter and rectifier with the load-independent operation. Note that $L_c = L_1 + 2L_x$, $L_t = L_2$, and $L_r = L_3 + 2L_x$. The rectifier parameters (i.e., L_f, L_x, and C_f) are also applied to the push–pull class E inverter to achieve the load-independent operation.

where

$$C_{2\text{eq}} = \frac{C_1 C_2}{C_1 + C_2}. \tag{37}$$

As L_1 and C_1 resonate at the operation frequency, the current through the transmitting coil can be obtained by Norton's theorem, i.e.,

$$\dot{I}_2 = \frac{\dot{V}_{\text{inv}}}{j\omega L_1} \tag{38}$$

which is irrelevant to load resistance. Therefore, the voltage gain is obtained by

$$G_{\text{mag}} = \frac{\dot{V}_{\text{rac}}}{\dot{V}_{\text{inv}}} = j\omega k_{23}\sqrt{L_2 L_3} \cdot \dot{I}_2 = \frac{k_{23}\sqrt{L_2 L_3}}{L_1}. \tag{39}$$

Thus, the compensation network realizes a load-independent voltage gain. The input impedance of resonant tank can be calculated by

$$Z_{\text{mag}} = R_1 + \frac{k_{\text{eq}}^2 \omega^2 L_1 L_2}{Z_{\text{lop2}}} \tag{40}$$

$$Z_{\text{lop2}} = R_2 + \frac{k_{23}^2 \omega^2 L_2 L_3}{R_3 + R_{\text{ac}}}. \tag{41}$$

Therefore, the input impedance of the resonant tank is ZPA regardless of load variation, which is preferable for the push–pull class E inverter.

2) Efficiency Improvement: As the resonant tank is separated into three compensated loops, the efficiency of each loop can be calculated individually, i.e.,

$$\eta_1 = \frac{Q_3}{Q_3 + Q_L} \tag{42}$$

$$\eta_2 = \frac{k_{23}^2}{k_{23}^2 + \frac{1}{Q_2}\left(\frac{1}{Q_3} + \frac{1}{Q_L}\right)} \tag{43}$$

$$\eta_3 = \frac{k_{eq}^2\left(\frac{1}{Q_3} + \frac{1}{Q_L}\right)}{k_{eq}^2\left(\frac{1}{Q_3} + \frac{1}{Q_L}\right) + \frac{k_{23}^2}{Q_1} + \frac{Q_3 + Q_L}{Q_1 Q_2 Q_3 Q_L}}. \tag{44}$$

Thus, the efficiency of the resonant tank is given by

$$\eta_{\text{mag}} = \eta_1 \eta_2 \eta_3. \tag{45}$$

To obtain the proper $L_{1\sim3}$, the resonant tank design can begin with selecting Q_L. Solving zero derivative of (45), i.e.,

$$\frac{d\eta_{\text{mag}}}{dQ_L} = 0 \tag{46}$$

gives

$$Q_{\text{Loptm}} = \frac{\sqrt{Q_3}\sqrt{k_{eq}^2 + \frac{1}{Q_1 Q_2}}}{\sqrt{Q_2 Q_3 k_{23}^2 + 1}\sqrt{\frac{k_{eq}^2}{Q_3} + \frac{k_{23}^2}{Q_1} + \frac{1}{Q_1 Q_2 Q_3}}} \tag{47}$$

where k_{eq} can be re-expressed according to (39), i.e.,

$$k_{\text{eq}} = \sqrt{\frac{k_{23}}{G_{\text{mag}}} \cdot \sqrt{\frac{L_3}{L_2}}} \tag{48}$$

where G_{mag} is given by specifications. k_{23} and $\sqrt{L_3/L_2}$ are limited by the size and transfer distance of coupling coils. Thus, L_3 and R_{ac} can be calculated according to the output specifications and Q_{Loptm}. The load resistance of the resonant tank (i.e., the input resistance of the push–pull class E rectifier) is approximately given by

$$R_{\text{ac}} = \frac{2R_{\text{dco}}}{G_{\text{rec}}^2} = 5.053074 \cdot R_{\text{dco}}. \tag{49}$$

The rated R_{ac} can be calculated by substituting R_{dco} with R_{r_d}, which is given by application specifications.

To figure out how much efficiency variation the load quality selection can cause, take a parameter set for example, where $Q_{1\sim3} = 300$, $k_{23} = 0.273$, and $k_{12} = 0.412$. The efficiency of the resonant is 95.3% at $Q_L = 1$, and reaches 97.1% at the optimal $Q_L = Q_{\text{Loptm}} = 3.05$. In other words, the resonant tank loss can be reduced by 39.4% after load quality optimization in this example. Thus, optimizing Q_L is critical for efficiency improvement of the resonant tank.

As shown in Fig. 8, an improved design flowchart is proposed for the resonant tank to adjust the parameters according to measurement. The FEM simulation is used for optimizing

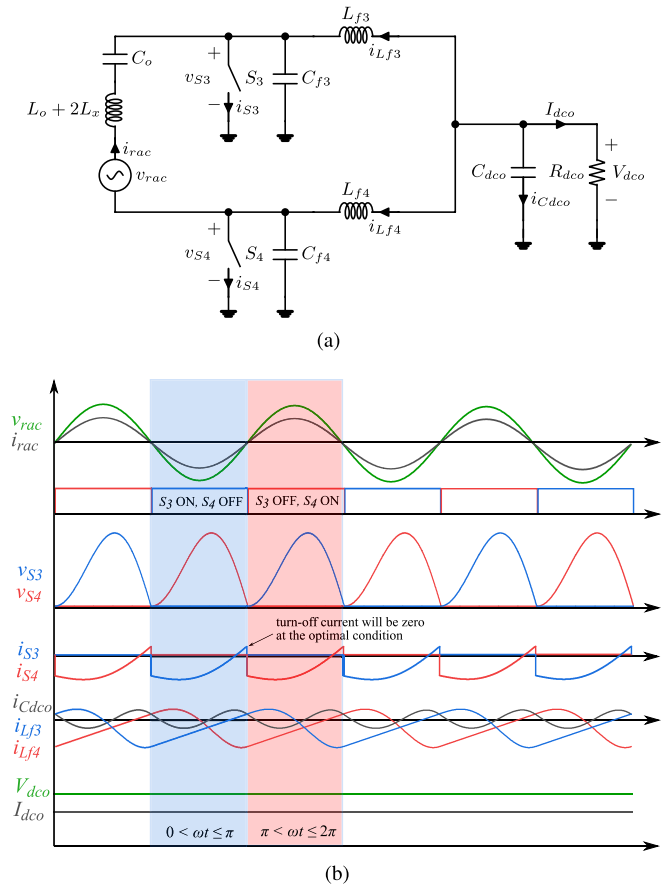

Fig. 6. Synchronous push–pull class E rectifier with the load-independent operation. The receiving coil combines the input inductance and the external inductance, i.e., $L_r = L_o + 2L_x$. The voltage source v_{rac} represents the induced electromotive force of the receiving coil by the mutual inductance of coupling coils. S_3 and S_4 operate differentially with 50% duty cycle. Due to the interleaving, the current ripple through C_{dco} is significantly reduced compared with that of the single-switch synchronous class E rectifier. (a) Equivalent circuit. (b) Key waveforms.

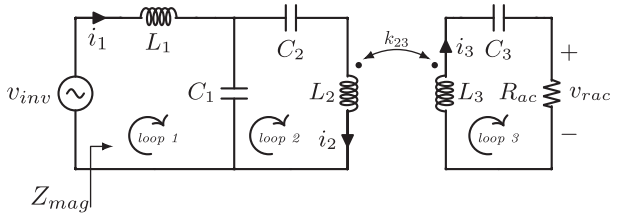

Fig. 7. Magnetic resonant tank formed by the coupling coils and the LCC-S compensation network. v_{inv} is the output voltage of the inverter. R_{ac} is the input resistance of the rectifier. Note that L_x is excluded from the analysis of the resonant tank.

the quality factors of the coils by adjusting the cross-sectional diameter and pitch of the wires. Then, the simulated results are used as the initial parameters for each adjustment loop. Finally, the improved design procedure makes the measured practical Q_L close to the optimal value as possible, and achieves the optimal efficiency of the resonant tank.

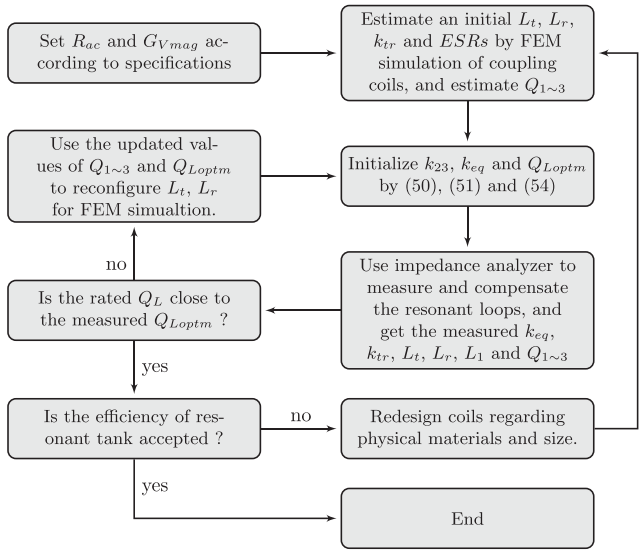

Fig. 8. Efficiency improvement of the LCC-S compensated resonant tank. Note that the tuned frequency of loop_1 and loop_3 should be adjusted according to (50). The values of L_2 and L_3 are obtained by $L_t = L_2$ and $L_r = L_3 + 2L_x$.

Since L_x of the push–pull class E rectifier/inverter is attached to the physical compensation network, the measured inductance values of resonant loops are $L_{\text{mes1}} = L_1 + 2L_x$, $L_{\text{mes2}} = L_t = L_2$, and $L_{\text{mes3}} = L_r = L_3 + 2L_x$. Thus, the expected tuned frequency of loop_1 and loop_3 should be adjusted to

$$f_{\text{mes1,3}} = \sqrt{\frac{L_{\text{mes1,3}} - 2L_x}{L_{\text{mes1,3}}}} \cdot f_{\text{op}} \tag{50}$$

where f_{op} is the operation frequency, L_{mes} is the measured inductance, and f_{mes} is the actual tuned frequency of resonant loops. Similarly, the coupling coefficient for resonant tank design is calculated by

$$k_{23} = k_{\text{tr}} \cdot \sqrt{\frac{L_r}{L_r - 2L_x}}. \tag{51}$$

Thus, the coupling coefficient of the practical coupling coils (k_{tr}) is different from that for resonant tank design (k_{23}).

IV. Example Design, Hardware Implementation, and Simulation

A. Design and Hardware Implementation

A prototype working at 6.78 MHz is built to achieve 48 to 48 V WPT for unmanned aerial vehicles. Table I illustrates the circuit parameters, which are obtained as follows.

1) Load-Independent Push–Pull Class E Rectifier and Inverter: As in Table I, the parameters of the inverter and the rectifier are obtained by (33)–(35). The theoretical rated power used for calculation is 220 W for both the inverter and the rectifier. As mentioned above, since the inverter can be regarded as a time-reversed synchronous rectifier, they use the same parameters to achieve load-independent operation.

Because of the conversation losses, the optimal condition, which achieves ZVS turn-ON and ZCS turn-OFF, is expected to

TABLE I
PARAMETERS OF PUSH–PULL CLASS E INVERTER AND RECTIFIER

	Circuit parameter	Value
Inverter	V_{dci}	48 V
	$L_{f1,2}$	644 nH
	L_x	171 nH
	$C_{f1,2}$	513 pF
Rectifier	R_{rd}	10.473 Ω
	$L_{f3,4}$	644 nH
	L_x	171 nH
	$C_{f3,4}$	513 pF
	Operation frequency	6.78 MHz
	Theoretical rated power	220 W
	GaN FET ($S_{1\sim4}$)	TP65H070LDG

TABLE II
PARAMETERS OF MAGNETIC RESONANT TANK

	Parameter	Calc.	Meas.[a]
Transmitting coil[b]	Outer diameter	150 mm	
	Number of turns	8	
	Pitch	4.5 mm	
	Inductance L_t	9.81 μH	10.46 μH
Receiving coil[b]	Outer diameter	100 mm	
	Number of turns	7	
	Pitch	4.2 mm	
	Inductance L_r	4.13 μH	4.15 μH
Compensation network	$L_1 + 2L_x$	2.01 μH	2.05 μH
	C_1	323.57 pF	322.70 pF
	C_2	62.93 pF	63.32 pF
	C_3	144.93 pF	145.18 pF
	Transfer distance	3 cm	
	Operation frequency	6.78 MHz	

[a] Measured by the impedance analyzer (4294A). [b] The coupling coils are made of the solid copper wires of 2-mm diameter.

be realized at the output power of about 200 W, which is lower than the theoretical rated output power.

2) Magnetic Resonant Tank: The resonant tank design can begin with the physical size of the coupling coils (i.e., L_t and L_r). In this example, both of the transmitting coil (15 cm by 15 cm) and receiving coil (10 cm by 10 cm) are circular spiral coils fixed in the square covers, and the transfer distance is fixed at 3 cm. Hence, the coupling coefficient is about 0.27 according to an 2D FEM (finite element method) simulation using cylindrical coordinate. In order to realize a conversation ratio of 1:1, the L_1, according to (39), is given by

$$L_1 = k_{23}\sqrt{L_2 L_3} \tag{52}$$

The ratio of L_2 to L_3 is about 0.386. The estimated $Q_{1\sim3}$ is 300. Thus, the optimal loaded quality factor of receiver loop can be calculated as $Q_{Loptm} = 3.047$.

As in Table II, the parameters of resonant tank can be obtained based on the design flowchart. The measured k_{eq} and k_{23} are 0.403 and 0.33, respectively. The measured $Q_{1\sim3}$ are 278, 216, and 290, respectively. Hence, the actual optimal loaded quality factor is about 2.688 corresponding to the load resistance $R_{\text{dco}} =$ 11.93 Ω, which is close to the rated load resistance in Table I.

3) Phase Detector: In a practical synchronous rectifier, the switches have to be driven with a proper phase shift from the input source. Thus, it requires a phase detector to synchronize the switching phase.

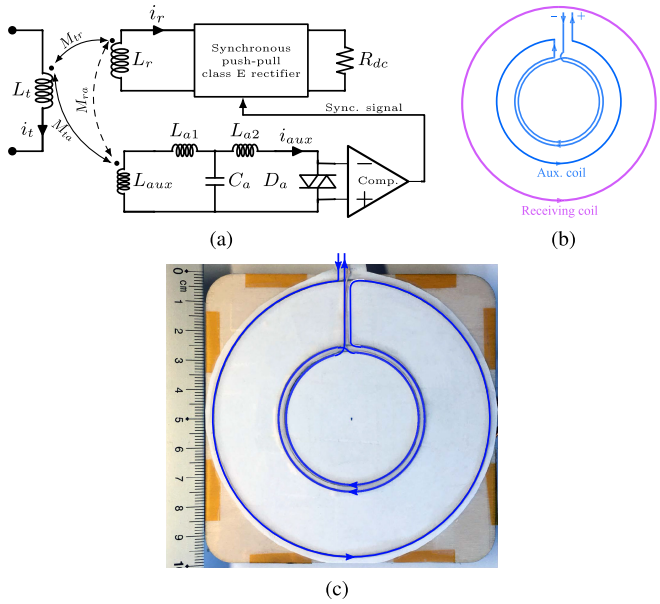

Fig. 9. Principle of the phase detector using the auxiliary coil. (a) Circuit schematic. (b) Coil structure of the receiver. (c) Hardware implementation of auxiliary coil. The transmitting coil L_t and the receiving coil L_r construct the magnetic link of the WPT system. The auxiliary coil comprises three turns, of which the winding direction of the outer turn is opposite to the inner two turns. The auxiliary coil is adjusted to be decoupled with the receiving coil (i.e., $M_{ra} = 0$), but maintaining a enough mutual inductance with the transmitting coil (i.e., $M_{ta} \neq 0$).

As analyzed in Section II, the load-independent operation achieves the ZPA input of the rectifier over the entire load range with a constant phase shift $\varphi = \pi$. Hence, the synchronous switches can be driven by a pulse with a constant phase shift from the input voltage. Naturally, the phase detection can be achieved without using current transformers or sensing the switch voltage, which may cause the unexpected switching phase shift due to load variation.

In this article, we use an alternative method to realize the phase detection. As illustrated in Fig. 9, the auxiliary coil is attached to the receiving coil and indirectly detects the phase of the induced voltage. It is decoupled with the receiving coil, but maintains a proper mutual inductance with the transmitting coil. Thus, the induced voltage $\dot{V}_{\text{aux}}$ can be expressed as

$$\dot{V}_{\text{aux}} = j\omega M_{\text{ta}}\dot{I}_t + j\omega M_{\text{ra}}\dot{I}_r. \tag{53}$$

Since $M_{\text{ra}} = 0$, the detected phase is irrelevant to the receiving coil current, avoiding the unexpected phase shift. The induced voltage of the auxiliary coil has a constant phase shift related to the driving phase of synchronous switches.

As in Table III, the wire diameter of the auxiliary coil is small enough to neglect the parasitic capacitance and ensure that the available operation frequency is much higher than the switching frequency.

As shown in Fig. 9(a), the auxiliary coil is compensated by a T-type LLC network, of which parameters meet

$$\frac{1}{\omega^2} = (L_{\text{aux}} + L_{a1}) \cdot C_a = L_{a2} \cdot C_a. \tag{54}$$

TABLE III
PARAMETERS OF AUXILIARY COIL

Parameter	Value
Number of turns	3
Outer diameter of turns	48 mm, 50 mm, 100 mm
M_{ta}	127 nH
L_{aux}	710 nH
Self-resonant frequency	46.5 MHz

As the auxiliary coil is decoupled with the receiving coil, the current source can be expressed as

$$\dot{I}_{\text{aux}} = -\omega^2 M_{\text{ta}} C_a \cdot \dot{I}_t. \tag{55}$$

Thus, the amplitude and phase are irrelevant to the variation of R_{dco}. We use a pair of antiparallel diodes to limit and shape the output voltage of the T-type network to a near-square waveform, of which the rise/fall time is shorter. Then, the comparator generates a synchronization signal sent to the driving circuit of the rectifier. Finally, the switch drivers can be triggered at the expected instant.

Using series capacitor is potential compensation for the auxiliary coil. However, the auxiliary will act as a voltage source, which cannot drive diodes due to the current limitation. Consequently, the movement of the receiver will result in a wide-range input voltage of the comparator when the diodes are removed. The trigger phase of the comparator will vary as the receiver moves. Moreover, the input voltage may exceed the withstand voltage and degrade the reliability of the signal processing circuit. Thus, it will be complicated for the series-capacitor compensation to obtain a reliable phase detector.

B. Circuit Simulation

The design example is simulated by MATLAB Simulink with the calculated parameters in the tables above. The synchronization circuit is also included in the schematic to verify the phase detector.

As in Fig. 10, a 50-μs delay is added before the driving pulses of synchronous switches are launched. Thus, the initial output voltage is built by the diode-based rectification. The delay is also implemented in the experimental prototype by using an RC delayer, and provides the following benefits.

1) The v_{ds} overshoot can be well suppressed since the diode-based rectification achieves the soft-switching naturally.
2) The auxiliary power supply for the driving circuit can be powered up adequately regardless of the load conditions, such as deeply discharged batteries.
3) The synchronous rectifier can be activated with a steady phase signal and thus avoiding the interference caused by power-ON transient.

The transient performance and voltage overshoot are related to the C_{dco}, which is a 4.7-μF capacitor used in the simulation. As in Fig. 10(a), a ten times load step is placed at 200 μs. The output voltage slightly varies from 48.3 to 48 V as the load resistance steps from 105 to 10.5 Ω. In other words, the output voltage varies lower than 0.6% as the output power steps from 10% to the rated value. Similarly, the variation is below 0.8% when the load steps from 10.5 Ω to no load. Therefore, the output voltage is nearly constant regardless of load variation. It also implies that the ZPA input impedance of the rectifier is realized since the system efficiency, the voltage gain, and the soft-switching of the inverter will be affected if the load of the resonant tank is not resistive. The simulation results match well with the theoretical analysis.

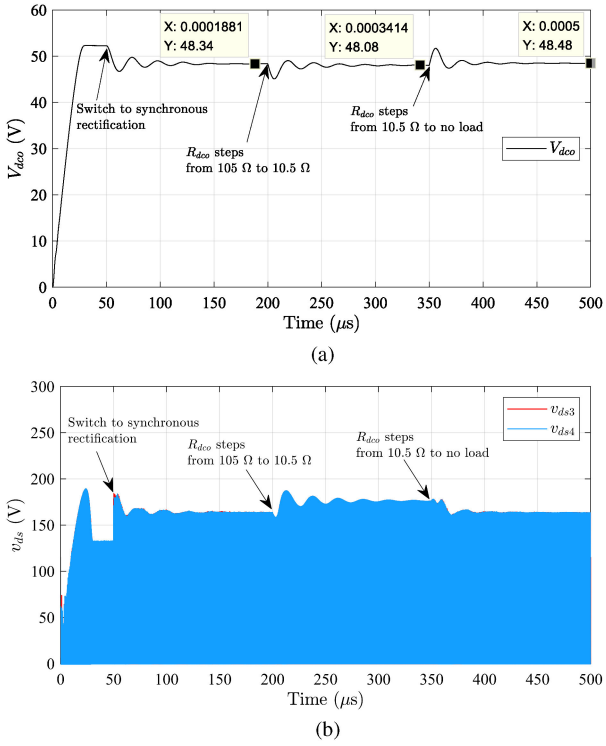

Fig. 10. Simulated output voltage and drain–source voltages of the synchronous push–pull class E rectifier with the load-independent operation. The output voltage varies lower than 0.8% over entire the load range without using close-loop control. (a) Output voltage. (b) Drain–source voltages.

Fig. 10(b) illustrates the drain–source voltage of the rectifier, i.e., $v_{ds3\sim4}$. The peak voltage slightly decreases as R_{dco} reduces. The waveforms present an envelope (i.e., outline) related to the transient state of V_{dco}, and they are unbalanced until the system reaches a steady state. This phenomenon will be even worse in practical systems due to parameter tolerances. Thus, the conventional phase-detection methods for single-switch rectifiers cannot be implemented directly for the synchronous push–pull class E rectifiers. By using the alternative method above, the phase signal is excited by the transmitting coil current. Thus, the driving pulses of synchronous switches are irreverent to the receiving coil current and the load resistance. Fig. 11 illustrates v_{ds} with a smaller time scale. The switches used in the simulation are ideal with linear parasitic capacitance, and the v_{ds} shape variation matches well with the theoretical curves in Fig. 2.

V. EXPERIMENT SETUP AND MEASUREMENT

A. Experiment Setup

Fig. 12 illustrates the experiment setup, which is built to verify the design methodology. As in Fig. 12(b), the circuit board of

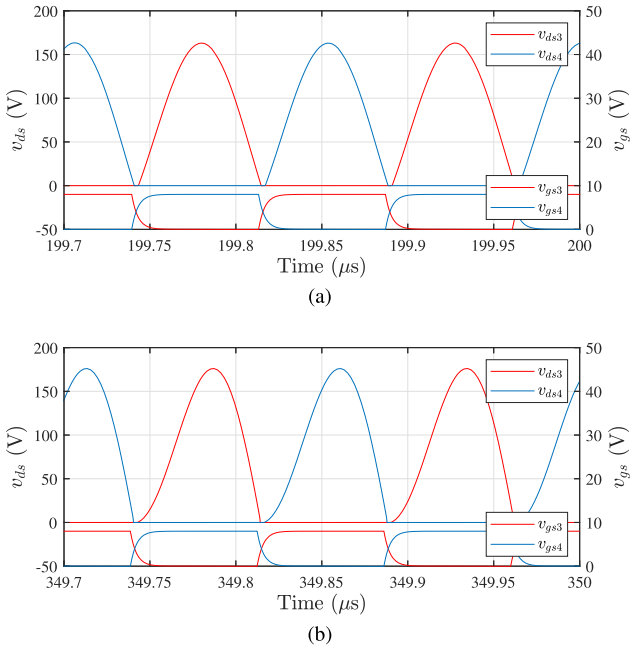

Fig. 11. Simulated drain–source voltages. The switches keep ZVS turn-ON as load varies. The ZCS turn-OFF is achieved at the rated load resistance. (a) $R_{\text{dco}} = 105\ \Omega$, $P_{o\_d} = 22.3$ W. (b) $R_{\text{dco}} = 10.5\ \Omega$, $P_{o\_d} = 219.9$ W.

the rectifier comprises the auxiliary power supply, the phase detector, and the rectification stage. $L_{f1\sim4}$ are constructed by helical air-core coils, of which ESRs are nearly constant over the load range. When the inverter is powered up, the rectifier operates at diode-based rectification mode until the output voltage of the auxiliary power supply is at steady state. An RC circuit (on the bottom side of the printed circuit board (PCB)) is implemented to set the delay before the synchronous driving pulses are enabled. The PCB layout is also implemented for the inverter, except its driving pulses that are generated by the signal generator. As in Fig. 12(c), the coupling coils are made of solid copper wires without using magnetic cores. Thus, the quality factors keep constant regardless of the exciting current. The auxiliary coil is decoupled with the receiving coil by adjusting the wire arrangement of the auxiliary coil. It connects to the phase detection circuit to drive the synchronous switches with a proper phase shift as illustrated in Fig. 13. Although the prototype is designed for fixed-position transfer, it is verified that the proposed phase detection is also applicable for the synchronous rectification of MHz-WPT systems with variable coupling. The switching phase keeps constant as the receiving coil moves horizontally with respect to the transmitting coil.

B. Measurement

Fig. 14 illustrates the measured V_{ds} and V_{gs} of the synchronous switches. The rectifier maintains ZVS over the designed load range. It matches well with the calculation and simulation in Figs. 2 and 11.

As in Fig. 14(a), the ZVS turn-ON is achieved, and the turn-OFF current is nonzero when the rectifier is at light load. The turn-OFF current decreases as the output power increases. As illustrated in

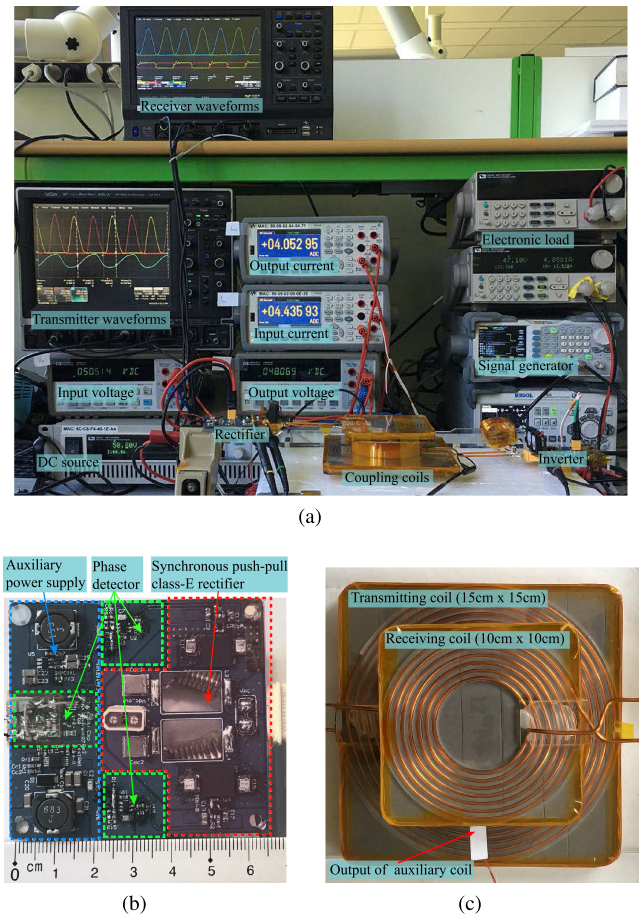

Fig. 12. Experiment setup. The transfer distance is fixed at 3 cm ($k_{tr} = 0.316$). The auxiliary coil is integrated on the receiving coil. (a) Measurement platform. (b) PCB of the active rectifier. (c) Coil structure.

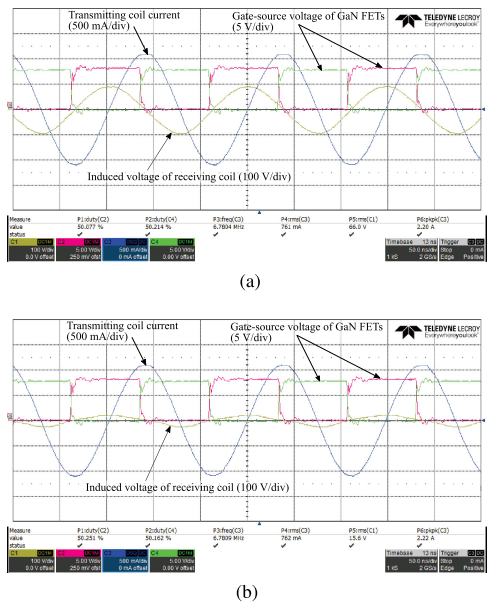

Fig. 13. Driving pulses of the synchronous switches, the transmitting coil current, and the open-load voltage of the receiving coil. The phase shift is adjusted according to the propagation delay of the driving circuit. (a) Aligned without position shift. (b) Misaligned with a 7-cm position shift.

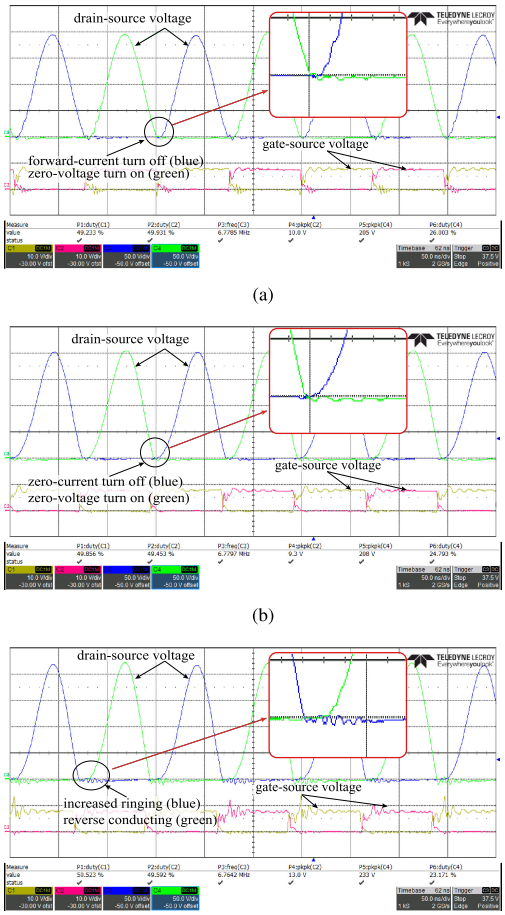

Fig. 14. Measured V_{ds} and V_{gs} of the synchronous switches versus load variation. The soft-switching is maintained over the designed load range, and it tends to be lost when the output power exceeds the rated value. (a) $R_{\rm dco} = 124.73\ \Omega$, $P_{o\_d} = 18.5$ W, $V_{\rm dco} = 48.02$ V. (b) $R_{\rm dco} = 11.84\ \Omega$, $P_{o\_d} = 194.1$ W, $V_{\rm dco} = 47.95$ V. (c) $R_{\rm dco} = 7.88\ \Omega$, $P_{o\_d} = 291.5$ W, $V_{\rm dco} = 47.94$ V.

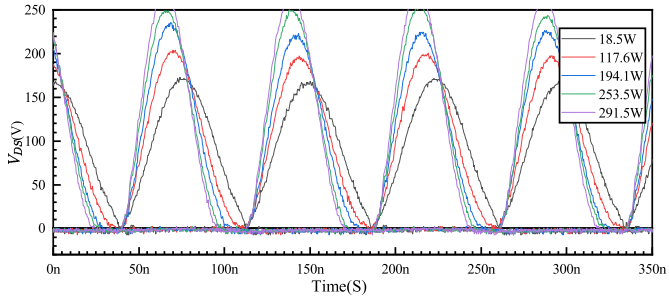

Fig. 15. Measured V_{ds} of the inverter versus load variation. The PCB layout of the rectifier is also implemented for the inverter, of which gate drivers are excited by the signal generator. The drain–source voltage varies as load varies, similar to the synchronous rectifier.

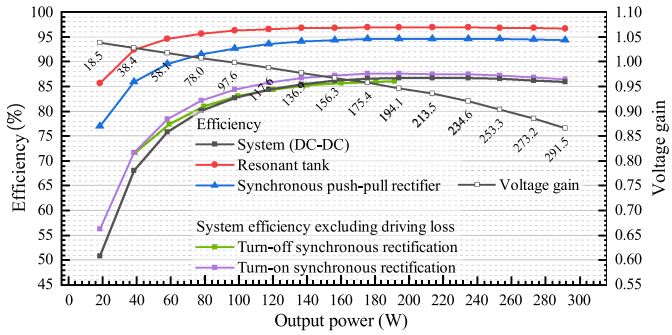

Fig. 16. Measured efficiency and voltage gain ($V_{\rm dco}/V_{\rm dci}$) versus output power (labeled). The output voltage is fixed at about 48 V by adjusting the input voltage. There is no external auxiliary dc source applied to the circuit board.

Fig. 14(b), both the ZVS turn-ON and ZCS turn-OFF are achieved when the output power is close to 200 W, which is the expected value achieving maximum efficiency. Besides, as illustrated in Fig. 14(c), the switches begin to conduct reversely at turn-OFF instant as the output power is above the rated value. Meanwhile, the switches are turning-ON before the drain–source voltage decreases to zero. Thus, the unreleased switch voltage will energize the resonance loop formed by the parasitic inductance and the parallel capacitance, resulting in a parasitic ringing phenomenon.

As in Fig. 15, the drain–source voltage of the inverter shows a similar variation to that of the rectifier. That means the load impedance of the inverter is resistive or near resistive.

Fig. 16 illustrates the measured efficiency and the voltage gain of the prototype. The efficiency of the resonant tank and the synchronous rectifier are estimated according to the measured quality factors and system efficiency. The measured peak system efficiency reaches 86.7% at 213.5 W ($R_{\rm dco} = 10.79\ \Omega$), of which the rectifier efficiency also reaches its peak value 94.6%, which is the same as at 194.1 W. The measured system efficiency is almost the same over the output power range from 194.1 to 253.3 W, and reaches its peak value at about 200 W, which matches well with the theoretical analysis. When the output power is above the rated value, the efficiency will not step down immediately. However, the temperature of the switches and the inductors will increase sharply as the output power increase to above 300 W. Eventually, the maximum output power is limited by thermal distribution. The measured gain decreases slowly as the output power increases due to the ESRs and nonlinear parasitic capacitance. The decrease accelerates when the output power is above 200 W. As a solution, feedback control, which is not discussed in this article, can be adopted to obtain a precise output voltage.

Fig. 16 also makes a comparison of the system efficiency with turn-ON and turn-OFF synchronous rectification. Turning OFF the synchronous driving pulses will result in a different diode-based rectification mode. The two rectification modes are different in terms of duty cycle, input impedance, voltage gain, drain–source voltage, etc. For the diode-based rectification, the driving circuit is not needed. When the output power is below 100 W, the system efficiency with diode-based rectification is slightly higher. However, when the driving loss (about 2 W) is excluded from the efficiency calculation, the system efficiency with synchronous rectification is always higher over the entire load range. Since the max surface temperature of the switches will exceed 100 °C,

the diode-based rectification is not able to output power above 200 W. Therefore, the synchronous rectification can output much higher power than the diode-based rectification.

VI. Conclusion

This article presents the analytical modeling and optimization of the load-independent synchronous class E rectifiers. An LCC-S compensated MHz-WPT topology, which comprises the push–pull class E inverter and rectifier with load-independent operation, is proposed to achieve the fully soft-switching and a nearly constant voltage gain over the entire load range. The improved design of the compensation network is also investigated to provide a design methodology of the proposed topology. The following conclusions can be made.

1) The ideal load-independent synchronous class E rectifiers realize the ZPA input impedance and the soft-switching over the entire load range with the constant voltage gain. The measured switching behavior matches well with the theoretical analysis.
2) The proposed optimal parameters of the synchronous class E rectifier realize both ZVS turn-ON and ZCS turn-OFFat the rated output power. The measured efficiency reaches its maximum value (94.6%) near the designed rated condition. It provides a preferable design method of the synchronous class E rectifiers.
3) The auxiliary coil can indirectly detect the optimal switching phase of the synchronous switches. Benefited from decoupling the auxiliary coil and receiving coil, the phase detection prevents mutual interference between the switches of the synchronous push–pull class E rectifier. It shows high stability in the MHz region without adding distinguishable loss.
4) The proposed improved design method of the LCC-S compensation network is conducive to improve the system efficiency. The measured system efficiency reaches its peak value (86.7%, 214 W) near the designed rated output power. It matches well with the theoretical optimal loaded quality.

References

[1] Z. Zhang, H. Pang, A. Georgiadis, and C. Cecati, "Wireless power transfer—An overview," *IEEE Trans. Ind. Electron.*, vol. 66, no. 2, pp. 1044–1058, Feb. 2019.

[2] C. Liu, C. Jiang, J. Song, and K. T. Chau, "An effective sandwiched wireless power transfer system for charging implantable cardiac pacemaker," *IEEE Trans. Ind. Electron.*, vol. 66, no. 5, pp. 4108–4117, May 2019.

[3] T. Kan, Y. Zhang, Z. Yan, P. P. Mercier, and C. C. Mi, "A rotation-resilient wireless charging system for lightweight autonomous underwater vehicles," *IEEE Trans. Veh. Technol.*, vol. 67, no. 8, pp. 6935–6942, Aug. 2018.

[4] Y. Dou, D. Zhao, Z. Ouyang, and M. A. E. Andersen, "Investigation and design of wireless power transfer system for autonomous underwater vehicle," in *Proc. IEEE Appl. Power Electron. Conf.*, Mar. 2019, pp. 3144–3150.

[5] X. Qu *et al.*, "Wide design range of constant output current using double-sided LC compensation circuits for inductive-power-transfer applications," *IEEE Trans. Power Electron.*, vol. 34, no. 3, pp. 2364–2374, Mar. 2019.

[6] M. Liu, M. Fu, and C. Ma, "Parameter design for a 6.78-MHz wireless power transfer system based on analytical derivation of class E current-driven rectifier," *IEEE Trans. Power Electron.*, vol. 31, no. 6, pp. 4280–4291, Jun. 2016.

[7] M. Liu, M. Fu, and C. Ma, "Low-harmonic-contents and high-efficiency class E full-wave current-driven rectifier for megahertz wireless power transfer systems," *IEEE Trans. Power Electron.*, vol. 32, no. 2, pp. 1198–1209, Feb. 2017.

[8] S. Aldhaher, D. C. Yates, and P. D. Mitcheson, "Load-independent class E/EF inverters and rectifiers for MHz-switching applications," *IEEE Trans. Power Electron.*, vol. 33, no. 10, pp. 8270–8287, Oct. 2018.

[9] K. Li, S. C. Tan, and R. S. Y. Hui, "Single-stage regulated resonant WPT receiver with low input harmonic distortion," *IEEE Trans. Power Electron.*, vol. 35, no. 7, pp. 6820–6829, Jul. 2020.

[10] K. Li, S.-C. Tan, and R. S. Y. Hui, "Single-switch-regulated resonant WPT receiver," *IEEE Trans. Power Electron.*, vol. 34, no. 11, pp. 10386–10391, Nov. 2019.

[11] H. Li, X. Zhang, M. Dai, H. Yang, Y. Wang, and D. Xu, "Design of a wireless power transfer system based on dual-class E self-resonant synchronous rectifier," in *Proc. 22nd Int. Conf. Elect. Mach. Syst.*, Aug. 2019, pp. 1–6.

[12] S. Aldhaher, D. C. Yates, and P. D. Mitcheson, "13.56 MHz 50 W load-independent synchronous class E rectifier using GaN devices for space-constrained applications," in *Proc. IEEE Wireless Power Transfer Conf.*, Jun. 2018, pp. 1–4.

[13] J. Song, M. Liu and C. Ma, "Class E active rectifier with controlled output voltage for MHz wireless power transfer," in *Proc. IEEE Trans. Power Electron.*, to be published, doi: 10.1109/TPEL.2020.3029525.

[14] M. Fu, Z. Tang, and C. Ma, "Analysis and optimized design of compensation capacitors for a megahertz WPT system using full-bridge rectifier," *IEEE Trans. Ind. Inform.*, vol. 15, no. 1, pp. 95–104, Jan. 2019.

[15] Y. Li, X. Ruan, L. Zhang, J. Dai, and Q. Jin, "Optimized parameters design and adaptive duty-cycle adjustment for class E dc–dc converter with on–off control," *IEEE Trans. Power Electron.*, vol. 34, no. 8, pp. 7728–7744, Aug. 2019.

[16] T. Nagashima, X. Wei, E. Bou, E. Alarcón, and H. Sekiya, "Analytical design for resonant inductive coupling wireless power transfer system with class-E inverter and class-DE rectifier," in *Proc. IEEE Int. Symp. Circuits Syst.*, May. 2015, pp. 686–689.

[17] S. Aldhaher, D. C. Yates, and P. D. Mitcheson, "A 25 W 27.12 MHz wireless power transfer system," in *Proc. IET Int. Conf. Power Electron. Mach. Drives*, Apr. 2016, pp. 1–4.

[18] S. Abbasian and T. Johnson, "High efficiency and high power GaN HEMT inverse class-F synchronous rectifier for wireless power applications," in *Proc. Eur. Microw. Conf.*, Sep. 2015, pp. 299–302.

[19] W. A. Nitz *et al.*, "A new family of resonant rectifier circuits for high frequency dc-dc converter applications," in *Proc. IEEE Appl. Power Electron. Conf.*, Feb. 1988, pp. 12–22.

[20] M. K. Kazimierczuk, "Class E low dv_D/dt rectifier," *IEE Proc. B Elect. Power Appl.*, vol. 136, no. 6, pp. 257–262, Nov. 1989.

[21] A. Reatti, M. K. Kazimierczuk, and R. Redl, "Class E full-wave low dv/dt rectifier," *IEEE Trans. Circuits Syst. I, Fundam. Theory Appl.*, vol. 40, no. 2, pp. 73–85, Feb. 1993.

[22] M. K. Kazimierczuk and J. Jozwik, "Class E zero-current-switching rectifier with a series inductor," in *Proc. 32nd Midwest Symp. Circuits Syst.*, Aug. 1989, vol. 2, pp. 788–791.

[23] J. A. Garcia and Z. Popovic, "Class-E rectifiers and power converters: The operation of the class-E topology as a power amplifier and a rectifier with very high conversion efficiencies," *IEEE Microw. Mag.*, vol. 19, no. 5, pp. 67–78, Jul./Aug. 2018.

[24] K. Jin, L. Gu, and J. Wang, "A 10-MHz resonant converter with a synchronous rectifier for low-voltage applications," *IEEE Trans. Power Electron.*, vol. 34, no. 4, pp. 3339–3347, Apr. 2019.

[25] Z. Zhang, X. Zou, Z. Dong, Y. Zhou, and X. Ren, "A 10-MHz eGaN isolated class-Φ_2 DCX," *IEEE Trans. Power Electron.*, vol. 32, no. 3, pp. 2029–2040, Mar. 2017.

[26] J. A. Santiago-Gonzalez, K. M. Elbaggari, K. K. Afridi, and D. J. Perreault, "Design of class E resonant rectifiers and diode evaluation for VHF power conversion," *IEEE Trans. Power Electron.*, vol. 30, no. 9, pp. 4960–4972, Sep. 2015.

[27] I. Ramos, M. N. Ruiz Lavín, J. A. García, D. Maksimović, and Z. Popović, "GaN microwave dc–dc converters," *IEEE Trans. Microw. Theory Techn.*, vol. 63, no. 12, pp. 4473–4482, Dec. 2015.

[28] X. Huang, Y. Kong, Z. Ouyang, W. Chen, and S. Lin, "Analysis and comparison of push–pull class-E inverters with magnetic integration for megahertz wireless power transfer," *IEEE Trans. Power Electron.*, vol. 35, no. 1, pp. 565–577, Jan. 2020.

[29] R. E. Zulinski and K. J. Grady, "Load-independent class E power inverters. Part I. Theoretical development," *IEEE Trans. Circuits Syst.*, vol. 37, no. 8, pp. 1010–1018, Aug. 1990.

Xiaosheng Huang (Member, IEEE) received the B.E. and Ph.D. degrees from Fuzhou University, Fuzhou, China, in 2009 and 2015, respectively.

He is currently an Associate Professor with the School of Electronic, Electrical Engineering and Physics, Fujian University of Technology, Fuzhou, China. He is also with the Fujian Provincial University Engineering Research Center for Industrial Automation, Fujian University of Technology. His current research interests include power conversion, high-frequency magnetics, wireless power transfer, and electromagnetic field analysis and applications.

Prof. Huang He is a member of the Magnetic Component Specialty Committee of the China Power Supply Society.

Yi Dou (Graduate Student Member, IEEE) received the B.S. degree in electrical engineering from Xi'an Jiaotong University, Xi'an, China, in 2016, and the M.Sc. degree in power electronics in 2018 from the Technical University of Denmark, Kongens Lyngby, Denmark, where he is currently working toward the Ph.D. degree.

His research focuses on design of high-frequency/very-high-frequency dc–dc converters, modeling for magnetic components, and modeling and optimization of MHz-range wireless power transfer systems.

Shuyi Lin received the B.E. and Ph.D. degrees from Fuzhou University, Fuzhou, China, in 2008 and 2014, respectively.

She is currently an Associate Professor with the School of Electronic, Electrical Engineering and Physics, Fujian University of Technology, Fuzhou, China. She is also with the Fujian Provincial University Engineering Research Center for Industrial Automation, Fujian University of Technology. Her current research interests include power conversion, high-frequency magnetics, and wireless power transfer.

Yuan Tian received the B.E. degree from Xiangnan University, Hunan, China, in 2018. He is currently working toward the M.E. degree with the School of Electronic, Electrical Engineering and Physics, Fujian University of Technology, Fuzhou, China.

His research interests include wireless power transfer and optimization of high-frequency magnetics.

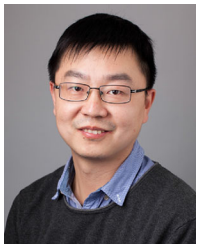

Ziwei Ouyang (Senior Member, IEEE) received the Ph.D. degree from Technical University of Denmark (DTU), Kongens Lyngby, Denmark, in 2011.

From 2011 to 2013, he was a Postdoc Researcher with DTU, where he was appointed as an Assistant Professor from 2013 to 2016, and has been an Associate Professor since April 2016. His research areas focus on high-frequency planar magnetics modeling and integration, high-density high-efficiency power converters, photovoltaic (PV) battery energy storage systems, and wireless charging. He has more than 70 high impact IEEE journal and conference publications, is a co-author of a book chapter on "Magnetics" in the *Handbook of Power Electronics* (Butterworth-Heinemann, 2018), and is the holder of eight international patents.

Dr. Ouyang was the Session Chair in some IEEE sponsored conferences and an Associate Editor for the IEEE JOURNAL OF EMERGING AND SELECTED TOPICS IN POWER ELECTRONICS. He was a recipient of Young Engineer Award at PCIM Asia 2014 and Best Ph.D. Dissertation of the Year Award 2012 in Technical University of Denmark. He was also the recipient of several Best Paper Awards in IEEE sponsored international conferences. He has been invited to give lectures in many universities, enterprises, and educational seminars and workshops around the world, including USA, Europe, and China.

Michael A. E. Andersen (Member, IEEE) received the M.Sc. and Ph.D. degrees in power electronics from the Technical University of Denmark, Kongens Lyngby, Denmark, in 1987 and 1990, respectively.

He is currently a Professor in power electronics with the Technical University of Denmark, where, he has been the Deputy Head of the Department of Electrical Engineering since 2009. He is the author or co-author of more than 300 publications. His research interests include switch-mode power supplies, piezoelectric transformers, power factor correction, and switch-mode audio power amplifiers.